Desalination and Water Treatment
www.deswater.com

doi: 10.5004/dwt.2017.0029

58 (2017) 19–34
January

Influence of the turbulence model choice on the simulation of active substance dispersion for the treatment of aquaculture pool invaded by algae

Amahoué François Moussoh[a], Anthony Biget[b], Cécile Lemaitre[a], Marie-Noëlle Pons[a,c,*], Jean-Pierre Leclerc[a,**]

[a]*Laboratoire Réactions et Génie des Procédés (UMR 7274 – CNRS) Université de Lorraine, ENSIC, 1, rue Grandville BP 20451, 54001 Nancy Cedex, France*
[b]*PROGEPI, 1, rue Grandville BP 20451, 54001 Nancy Cedex, France*
[c]*LTER, Zone Atelier du Bassin de la Moselle, Laboratoire Réactions et Génie des Procédés, (UMR 7274-CNRS) Université de Lorraine, 1, rue Grandville, BP 20451, 54001 Nancy cedex, France, Tel. +33 383175277;*
email: marie-noelle.pons@univ-lorraine.fr (Marie-Noëlle Pons)
***INRS, 1 rue du Morvan, CS60027, 54519 Vandœuvre cedex, France*

Received 8 January 2016; Accepted 19 May 2016

ABSTRACT

The effect of the choice of turbulence models on the simulation by a computational fluid dynamics (CFD) code of flow patterns in aquaculture ponds to optimize the dispersion of an active substance against algae has been investigated. The selected pond has a length of 30.5 m, a width of 7.32 m, and a variable depth (1.05 m upstream and 1.65 m downstream) along a bottom slope of 1.62% with one inlet and one opposite outlet. Five turbulence models, available in Fluent®, have been tested: Standard k-ε (Sk-ε), Re-Normalization Group (RNG) k-ε, Realizable k-ε (Rk-ε), Reynolds Stress Model (RSM), and Transition SST (Shear Stress Transport). The contours of flow velocity magnitudes and the velocity vectors were examined and differences have been highlighted between these models. The comparison of velocity profiles at different locations in the pond shows that the choice of the model affects the simulated hydrodynamic behavior and consequently the prediction of the active substance dispersion. These differences are also affecting the residence time distribution.

Keywords: Algae; CFD simulation; Residence time distribution; Turbulence models; Water treatment; Fluent®

1. Introduction

A fish pond is defined as an artificial structure used for the farming of fish. In Europe and around the world, fertilizers or hormones [1] are often used to improve the yields of fish ponds. Fertilizer inputs and organic waste from fish metabolism contribute to eutrophication of fish ponds [2]. Eutrophication is a process of nutrient overenrichment of a water body [3], resulting in an increase of the biological productivity (growth of algae). In the past, the typical treatment to remove the undesired algae consisted in dumping large quantities of copper sulfate in the water causing not only the death of algae but unfortunately enormous damage to aquatic ecosystems. The state of the art regarding methods of control against plant invasions in aquatic environments has led to carry out research to find new treatments. The global objective of the present study is to develop an innovative process to locate the areas to be treated and effectively target aquatic plants to treat. Then, an optimal treatment based on acceptable concentration of product could be designed that could kill only the targeted invasive plants. The treatment of these fish ponds overrun by invasive aquatic plants (algae, duckweed, and cyanobacteria) requires the understanding of the flow behavior.

* Corresponding author.

The development of numerical models is necessary [4,5] because of the difficulty to understand pond hydrodynamic phenomena by simple observation. The goal will be to get the best compromise between the reliability of the information provided by the model, its complexity, and the computation time. To model the hydrodynamics of a fish pond, the analysis of various parameters (mesh, boundary conditions, and types of models) allows us to establish preferential conditions for an efficient and accurate simulation.

There are several types of aquaculture ponds whose geometry may vary from one configuration to another. However, in general, fish ponds are characterized by vertical flow, recirculation, dead zones and by the fact that the inward flow along the pond inlet or bottom contributes to short-circuiting [6,7]. Most works dealing with flow behavior in ponds were performed in two main geometries: circular ponds [8–10] and rectangular ones [11–16]. In order to ensure optimal fish culture conditions, and easier management of fish farms in case of ponds threatened by pollution and invasive species, the selection of pond geometry is important [14]. An aquaculture circular pond provides a more homogeneous distribution of dissolved oxygen and rapidly flushes wastes [8,17]. Rectangular ponds are easier to clean, but there present frequently poor mixing and dead zones, which favors the accumulation of bio-solids (fecal waste materials or nutrients) on the bottom of the pond and therefore eutrophication [14]. The CFD-based simulation of aquaculture ponds have been used to describe water flow in circular and rectangular tanks [18–24].

A rectangular fish pond was used to study the influence of the turbulence models in the fish pond flow simulation. According to Food and Agriculture Organization (FAO) of the United Nations, the average depth of a rectangular fish pond should be between 0.5 and 1.5 m with a smooth slope. The regime in the inlet pipe, whose diameter is in the range 0.1 to 0.2 m, is turbulent, with a Reynolds number of around 60,000. Inside the pond, the local Reynolds number varies between about 100 and 36,000. This large variation of the flow regimes inside the volume (laminar, transition and turbulent flow) makes that the simulation of the flow behavior using CFD is not straightforward despite the apparent simplicity of the system.

The numerical simulation of the fish pond flow could be validated through the inspection of the numerical residence time distribution (RTD) curve. However, it is often difficult to set up such experiments and as a paradox most of the papers do not compare several models and/or numerical RTD. In particular the choice of turbulence models differs from one researcher to another and this makes the comparison between results difficult. Table 1 shows the common turbulence models that have been used by different

Table 1
Models tested in previous studies of the literature

Authors and characteristic of aquatic environment used	Models tested by the authors							
	Sk-ε	RNG k-ε	Rk-ε	RSM	Sk-ω	SST	k-kl-ω	TSST
Alvarado et al. (2013) [25] Wastewater pond Area = 70 000 m^2 Depth = 1.7 m Average flow = 1.2 m^3/s	●							
Wu and Chen (2006) [26] Anaerobic lagoons Area = 5,670 m^2 Depth = 4.3 m Inlet flow = 0.01 m^3/s					●	●	●	●
Stovin et al. (2008) [27] Storage tank Area = 0.76 m^2 Depth = 0.45 m Inlet flow = 0.005 m^3/s		●		●				
Tarpagkou et al. (2013) [28] Sedimentation tank Area = 24 m^2 Depth = 0.8 m Flow rate = 0.007 m^3/s	●							
Hreiz et al. (2014) [29] Pond used for algaculture Area = 67. 09 m^2 Depth = 0. 15–0.4 m Velocity = 0.15–0.4 m/s			●					

● = The model is used by the author.

researchers. Alvarado et al. [25] used Standard k-ε (Sk-ε) for the simulation of the flow in a waste stabilization pond. The comparison of numerical and experimental RTD curves showed that the maximum peak amplitude of experimental tracer normalized concentration is lower than in the simulation. The mean residence time obtained with the Sk-ε model was around 35% lower than the experimental time. The authors explained that this was due to short-circuiting phenomena and dead zones within the pond but the choice of the Sk-ε model could also be part of the explanation of this discrepancy. Wu and Chan [26] have tested the k-ω models family (Sk-ω, SST k-ω, TSST and k-kl-ω) in order to simulate the low velocity behavior and fluid recirculation inside a rectangular lagoon. It appears that the Transition SST model simulates a little better the water flows than the three other models based on numerical and theoretical residence time criteria. According to the authors, the simulated mean residence time (MRT) at the outlet is very close to the theoretical MRT within a 1.2% error margin. Apart from the comparison of MRT, it would be preferable to compare the shape and the RTD curves since the MRT should be independent of the turbulence model.

The scale of the fish pond configuration also plays an important factor in the flow behavior. Stovin et al. [27] modeled the dispersion parameters in a laboratory storage tank using a Re-Normalization Group (RNG) and a Reynolds Stress Model (RSM). Their results showed that the RTD curve of RSM model was almost superimposed with measured RTD curve. They noticed a slight lag between the RTD curve simulated with the RNG model and the one obtained experimentally. Furthermore, the maximum peak amplitude of the concentration was less for the RNG model. However, they showed that the MRT simulated with RNG flow model gives a discrepancy of 3%, unlike the RSM turbulence model which yielded a value of MRT 18% higher than the expected value.

This study aims at testing, on a numerical basis various closure models from literature in order to select the most appropriate one for modeling an aquaculture pond. This optimal closure model will be later used to predict the outcome of tracing experiments on real ponds.

2. Materials and methods

2.1. Simulated fish pond configuration

Fig. 1 shows a three-dimensional (3D) geometry of the simulated fish pond. The pond has a volume of 301.4 m^3 with dimensions 30.5 x 7.32 m and non-constant depth (1.05 m upstream and 1.65 m downstream) along a bottom slope of 1.62%.

Water enters and exits the fish pond through a rectangular pipe of dimensions 0.4 x 0.2 m corresponding to a hydraulic diameter of 0.2 m and a volumetric steady flow rate of 0.024 m^3/s.

The pond inlet is located at the maximum pond water level (horizontal free surface) and the outlet at 0.2 m from the sloped bottom.

The regime in the inlet pipe is turbulent, with a Reynolds number of 60,000. Inside the pond, laminar and turbulent régimes coexist since the local Reynolds number varies between 115 and 36,000.

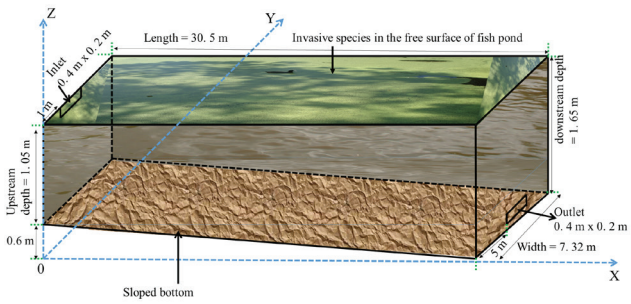

Fig. 1. 3D geometry of the simulated fish pond.

2.2. CFD modeling

The hydrodynamic flow of the fish pond is studied as a monophasic flow. The three dimensional CFD simulations of fish pond flow is investigated (Fig. 1) by using ANSYS Fluent® 14.5 on an Intel Core computer, with a 3.20 GHz i3 4-processor and 4 GB RAM. Five turbulence models (RSM, Rk-ε, RNG k-ε, Sk-ε, and TSST models) were tested in order to study their effects on the pond hydrodynamic behavior.

2.3. Governing equations

2.3.1. Fluid motion

The modeling of a turbulent incompressible flow is generally based on the laws of mass conservation (continuity) and momentum. The equations governing the water flow are the well-known Reynolds-Averaged Navier–Stokes (RANS) equations. The studied pond is shallow (Fig. 1). We assume that the water is an incompressible Newtonian fluid [28–30] with a constant density and that it undergoes a steady-state flow, which allow us to simplify the general Navier–Stokes equations [22]. The water flow model that contains basically the equations of continuity (1) and momentum (2) is expressed in tensor notation, with the Einstein summation convention, as follows:

$$\frac{\partial \rho u_i}{\partial x_i} = 0 \tag{1}$$

$$U_j \frac{\partial U_i}{\partial x_j} = -\frac{1}{\rho}\frac{\partial p}{\partial x_i} + \frac{\partial}{\partial x_j}\left(v\left(\frac{\partial U_i}{\partial x_j} + \frac{U_j}{\partial x_i}\right) - \overline{u_i' u_j'}\right) \tag{2}$$

where x_i (or x_j) is the Cartesian coordinate; U_i is the mean flow velocity; u'_i (or u'_j) is the turbulent velocity fluctuation; u_i ($u_i = U_i + u'_i$) is the instantaneous velocity in the x (longitudinal), y (lateral), and z (vertical) directions; ϱ is the density of water; v is the kinematic viscosity; p is the static pressure and $\overline{u_i' u_j'}$ is the component of the Reynolds-stress tensor. A turbulence model must be used to solve for this last term that is initially unknown.

2.3.2. Turbulence models

Further information about the equations of the five tested models is available in the references listed thereafter.

2.3.2.1. Sk-ε model [31–33]

The Reynolds stresses could be linked to the mean rate of deformation. Sk-ε model (two-equation model) is based on the Boussinesq approximation assuming that the turbulence regime is fully established in the whole area and the effects of molecular viscosity are negligible compared to those of the turbulent viscosity (away from the walls). The Reynolds-stress in the mean flow is written as follows:

$$\overline{-\rho u_i' u_j'} = \mu_t \left(\frac{\partial U_i}{\partial x_j} + \frac{\partial U_j}{\partial x_j} \right) - \frac{2}{3} \rho k \delta_{ij} \tag{3}$$

where μ_t, a scalar property is called eddy viscosity; k is the turbulent kinetic energy; δ_{ij} is the Kronecker delta.

The turbulent viscosity (or eddy viscosity) is calculated by the model involving the turbulent kinetic energy (k) and the turbulent dissipation (ε) as follows:

$$\mu_t = \rho c_\mu \frac{k^2}{s} \tag{4}$$

where C_μ is a constant equal to 0.09 (empirical default value used in the CFD code Fluent).

$$k = \frac{1}{2} \overline{u_i' u_i'} \tag{5}$$

$$\varepsilon = v \overline{\frac{\partial u_i \partial u_i}{\partial x_j \partial x_j}} \tag{6}$$

The two transport equations that are used in Sk-ε model are expressed as follows.

$$\frac{\partial(\rho k)}{\partial t} + \frac{\partial(\rho k u_i)}{\partial x_i} = \frac{\partial}{\partial x_j} \left(\frac{u_t}{\sigma_k} \frac{\partial k}{\partial x_j} \right) + 2\mu_t E_{ij} E_{ij} - \rho\varepsilon \tag{7}$$

For the dissipation (ε),

$$\frac{\partial(\rho s)}{\partial t} + \frac{\partial(\rho s u_i)}{\partial x_i} = \frac{\partial}{\partial x_j} \left(\frac{u_t}{\sigma_\varepsilon} \frac{\partial_\in}{\partial x_j} \right) + C_{1s} \frac{s}{k} 2\mu_t E_{ij} E_{ij} - C_{2s} \rho \frac{s^2}{k} \tag{8}$$

where E_{ij} is the component of a rate of deformation.

The standard values of the Sk-ε model constants used for the water flow simulation are indicated in Table 2.

This model is widely used in the water flow simulation. It is robust because of low cost of calculation time, sufficiently precise and validated for a wide range of turbulent flows. However, it presents some limitations like an excessive (unphysical) production of turbulenty kinetic energy (k) in regions with large strain rate (for example, near a stagnation zone), resulting in very inaccurate model predictions. The results strongly depend on these empirical constants (Table 2) presenting one of the weaknesses of this model.

Table 2
Constants of the Sk-ε model

C_μ	σ_k	σ_ε	$C_{1\varepsilon}$	$C_{2\varepsilon}$
0.09	1.0	1.3	1.44	1.92

The Sk-ε model was modified while making improvements that led to the development of the RNG k-ε based on the theory of renormalization group and the Rk-ε model that relies primarily on a new equation in the turbulent dissipation (ε).

2.3.2.2. Rk-ε model [34–36]

The Rk-ε model differs from the Sk-ε in that has a new formulation for the turbulent viscosity (μ_t) and a new equation for the turbulent dissipation (ε). Dissipation rate (ε) equation is derived from the mean-square vorticity fluctuation, which is fundamentally different from the Sk-ε model.

The turbulent viscosity is determined according to the Eq. (4) but here C_μ is no longer constant. C_μ is dependent on other parameters such as the average values of flow stresses, rotations, and turbulence fields (k and ε). The term "Realizable"' is used to explain that the model satisfies certain mathematical constraints on the Reynolds stresses, consistent with the physics of turbulent flows. Compared with the Sk-ε model, the Rk-ε model provides superior performance for flows involving rotation, separation, and recirculation. One of the limitations of the Rk-ε model is that it seemed less suitable in areas where the local flow Reynolds number is low (almost stagnant zones) .

2.3.2.3. RNG k-ε [23,32,37,38]

The RNG model uses equations that are similar to those of the Sk-ε model. However, the constants of the RNG k-ε model are evaluated by theoretical calculations and not empirically. The constants in the RNG k-ε are derived analytically using group renormalization theory, which is a complex mathematical procedure that makes the description of the system dependent on the scale of variations of local Reynolds number. Compared to Standard k-ε model, the main improvement is the addition of an extra term in the "ε" equation that improves the accuracy for rapidly strained flows. In rate dissipation equation (8), C_{1s} is replaced by C'_{1s} depending on the strain rate η making it less diffusive. C_{1s} is included in the new term C_{1s} (that is determined during calculation).

$$C'_{1s} = C_{1s} - \frac{\eta \left(1 - \frac{\eta}{\eta_0} \right)}{1 + \beta \eta^s} \tag{9}$$

$$\eta = \frac{k}{s} (2S_{ij}^2)^{1/2} \tag{10}$$

$$S_{ij} = \frac{1}{2} \left(\frac{\partial U_i}{\partial x_j} + \frac{\partial U_j}{\partial x_i} \right) \tag{11}$$

where S_{ij} is a mean rate of strain tensor

The standard values of the constants of the RNG k-ε model used for the water flow simulation are indicated in Table 3. This model has wider applicability than the Sk-ε model. In particular the effects associated with low Reynolds are taken into account and laminar behavior can be predicted.

Table 3
Constants of the RNG k-ε model

β	η_0	σ_k	σ_ε	$C_{1\varepsilon}$	$C_{2\varepsilon}$
0.015	4.38	0.085	0.7179	1.42	1.68

2.3.2.4. RSM [39,40]

The Reynolds Stress Model (RSM) is a higher level, elaborate turbulence model that is usually called a second-order closure. It does not use the isotropic eddy-viscosity concept but consists in transport equations for the individual Reynolds stresses, together with an equation for the dissipation rate. This means that seven additional transport equations must be solved in 3D water flow simulation. The RSM accounts for the effects of streamline curvature, swirl, rotation, and rapid changes in strain rate in a more rigorous manner than two-equation (Rk-ε, RNG k-ε, Sk-ε) models. This model seems to fit the pond flow simulation of flows of surface waters with a simplified or complex geometry in the local zone of high Reynolds number. The computational time cost is higher than in the previously described models.

2.3.2.5. SST Transition model [41]

The Transition SST model was developed by Menter et al. [41]. It is a four-equation turbulence model based on the coupling of the SST k-ω (derivative of the k-ω model) transport equations with two other transport equations, one for the intermittency and one for the transition onset criteria, in terms of momentum-thickness Reynolds number. The turbulent kinetic energy (k) of this model is similar to the turbulent kinetic energy equation of the Sk-ε model, and the specific dissipation (ω) is thought as the ratio of ε. The specific dissipation ($\omega = \frac{\varepsilon}{k}$) should be interpreted as the inverse of timescale at which dissipation occurs. The turbulent viscosity (μ_t) is modified to account for the transport of turbulent shear stress. It is calculated from:

$$\mu_t = \frac{k}{\omega} \tag{12}$$

This model is adapted for low Reynolds number flows. Compared to the Sk-ε, RNG k-ε and k-ε model, its computational time cost higher.

Further information about the equation of the Transition SST model is detailed in Menter et al. [41].

2.3.3. Simple strategy for the preliminary selection of the models

The preliminary selection of the five turbulence models in our study is based on previous studies, models assumptions and the main hydrodynamics behavior that the models can predict better.

Fig. 2 shows some simple strategy adopted for the models selection. We have established at least three main criteria for the preliminary selection of our studied models:

- A criterion based on the physical analysis of local flow behavior
- A criterion based on the mathematical formulation of models (model parameters).
- A criterion based on the computation time

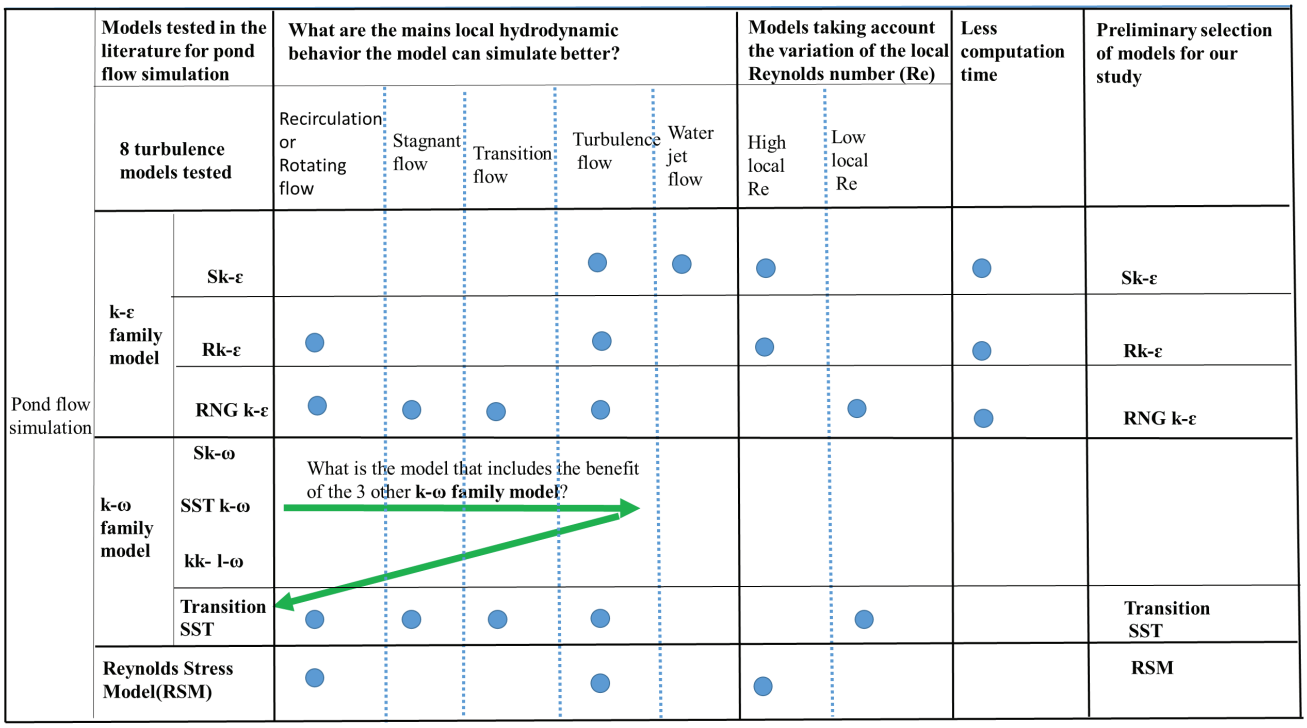

Fig. 2. Simple strategy for the preliminary selection of turbulence models.

2.4. Species transport equation without reaction

The modeled tracer concentration with the convection and diffusion equation without reaction is [26,42–46]:

$$\frac{\partial(\rho Y_i)}{\partial_t} + \nabla.(\rho \vec{u} Y_i) = -\nabla \vec{j_t} \quad (13)$$

where ϱ is the local density of the mixture, Y_i is the local mass fraction of each species, *u* refers to the velocity. $\vec{J}_i$ is the mass diffusion flux of species i computed in the following form in Fluent [42]:

$$\vec{j_1} = -(\rho D_{i,m} + \frac{\mu_t}{Sc_t})\nabla Y_i \quad (14)$$

$D_{i,m}$ is the diffusion coefficient for species *i* in the mixture, μ_t is the turbulent viscosity, Sc_t is the turbulent Schmidt number [47].

$$Sc_t = \frac{\mu_t}{\rho D_t} \quad (15)$$

D_t is the turbulent diffusion.

The species concentration is defined as a mass fraction for the simulation. For the boundary condition of the simulated species dispersion, the inlet mass fraction of injected tracer is equal to 1 at the initial time (t = 0 second) [48,49]. The mass fraction of the last species is computed by subtracting the total of the specified mass fractions from 1 [42]. The outflow and symmetry boundaries conditions are, respectively, applied at the outlet and the free surface. Zero concentration is set for all walls [42,48].

2.5. Method used to simulate tracer transport

The RTD is calculated using Species Transport method [25]. The tracer is modeled as a species. The numerical tracing involves injecting the simulated tracer at the inlet and monitoring the variation of his concentration at the outlet. The concentration of a tracer has no significant effect on the water flow fields because they have the identical properties. First, the water flow equations are solved using a steady-state approach. Second, the species transport equation is solved as an unsteady simulation using the computed water flow solution. To study the influence of turbulence model on the local dispersion of the active substance, we create a few points or surfaces in any position inside the pond in order to inject locally or monitor the concentration of the substance within the pond.

2.6. Boundary conditions for flow simulation

A velocity-inlet boundary condition is used at inlet. The velocity magnitude of 0.3 m/s is indicated in the longitudinal position of the inlet with a hydraulic diameter of 0.2 m. The turbulence intensity (I) is of 4%, where $I = 0.16.(Re)^{-0.125}$ [50] and Re is the Reynolds number. The outlet is indicated as the outflow boundary condition [37]. A no-slip wall condition is used for the pond bottom and for the other walls. At the free surface, a symmetry boundary condition is used [50,51]. The effect of the presence of fish on flow patterns and sediment transport is neglected [20].

2.7. Simulation procedure

We used the Cartesian method "Cut-Cell" [52–54] to generate a uniform Cartesian grid on almost the entire area. The mesh is composed of 99% of hexahedral cells and 1% of prismatic meshes. These meshes have a regular shape and allow to minimize numerical diffusion and reduce computation time. We have tested several size of meshes giving 833,242, 670,352 and 335,854 cells for the five models used. All tested meshes have orthogonal quality [55] with the mean ratio equal to 0.99. The mesh independence study was performed in order to examine their effect on simulation results for all models used. The coincidence of simulation results obtained with the varying mesh size attests that the results are independent of the mesh [42,56–59]. The water flow is simulated in steady state and the species transport equations are computed in unsteady state. We have used Standard Scheme for the Pressure interpolation. The algorithm SIMPLE (Semi Implicit Method for Pressure Linked Equations) was used for the pressure-velocity coupling. For the gradient, Green Gauss Cell based method was used. The discretization scheme used is the first-order upwind to get convergence first and the refinement of the results at the second order or QUICK (Quadratic Upwind Interpolation for quadrilateral or hexahedral mesh). Enhanced wall treatment was used for the turbulence models needed the wall treatment [60,61]. In this study the residuals (convergence criterion) were set to be inferior to 10^{-6} for all solved equations in order to improve solution accuracy [22,42]. For the mass flow criterion the net imbalance between the inlet and outlet fluxes was found to be less than 0.05 % for mass, momentum, and scalar balances [22,42].

3. Results and discussions

3.1. Influence of turbulence models on 3D

3.1.1. Visualization on several planes

Several planes are selected in order to visualize the effect of the turbulence models on the 3D flow (Figs. 3a and 4a).

The water flow inside the pond is mainly characterized by convective flow, a backward flow and a recirculation flow as illustrated in Figs. 3 and 4. Fig. 3 shows the effect of the RSM (a), Rk-ε (b), RNG k-ε(c), Sk-ε (d), and TSST (e) models on the velocity flow at the free surface of the pond. Fig. 4 shows the comparison of velocity contours and vectors at axial, transverse, and vertical planes between the five turbulence models RSM (a), Rk-ε (b), RNG k-ε(c), Sk-ε (d), and TSST (e). The flow visualization showed in Figs. 3 and 4 reveal that global hydrodynamic behavior is similar for these five turbulence models. Inside the pond, the mean flow velocity obtained is about 0.02 m/s for all turbulence models aside from the model Sk-ε (d) giving a mean velocity of 0.026 m/s whose deviation is estimated at 23% compared to the four other models. Globally, the direction of velocities vectors shows that the flow is independent of the slope of pond bottom as shown in Figs. 3 and 4. It is divided into three main zones inside the pond, as illustrated in Fig. 5. Fig. 5 shows the schematization of the global hydrodynamic behavior simulated by the five models.

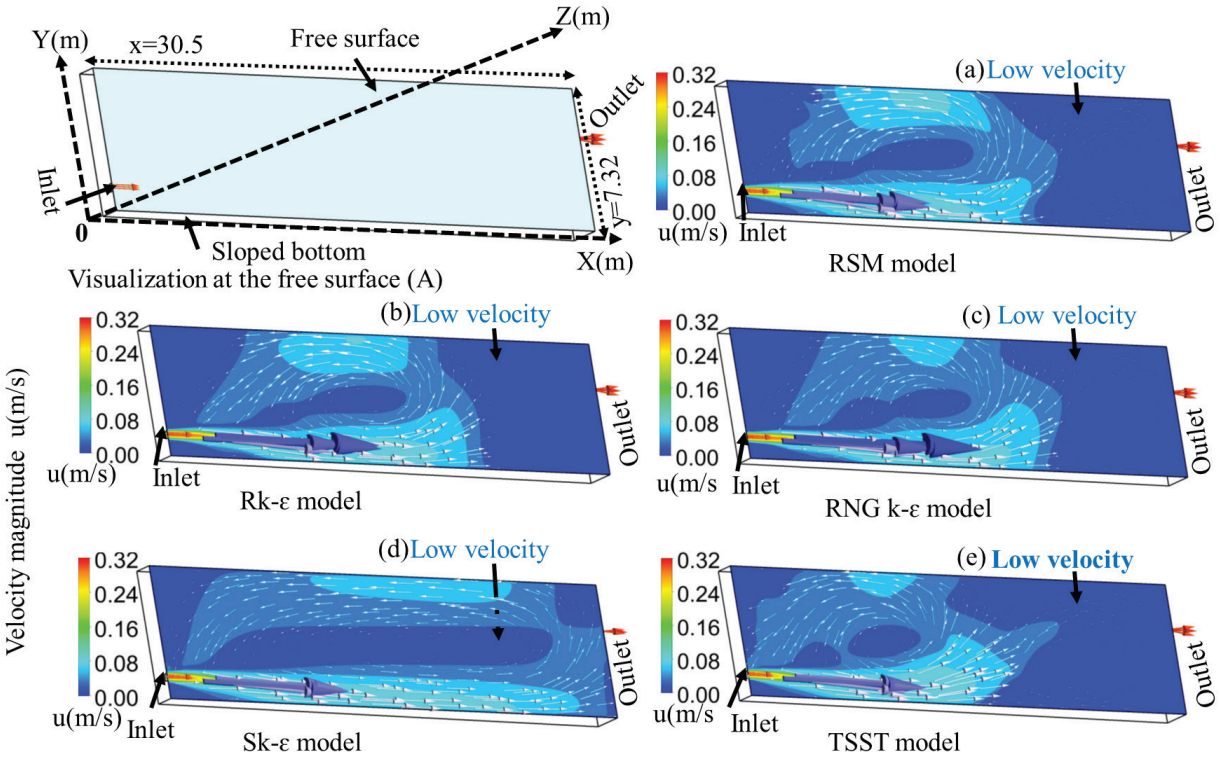

Fig. 3. Comparison of velocity contours and vectors at the free surface. (a) RSM , (b) Rk-ε, (c) RNG k-ε, (d) Sk-ε and (e) TSST models.

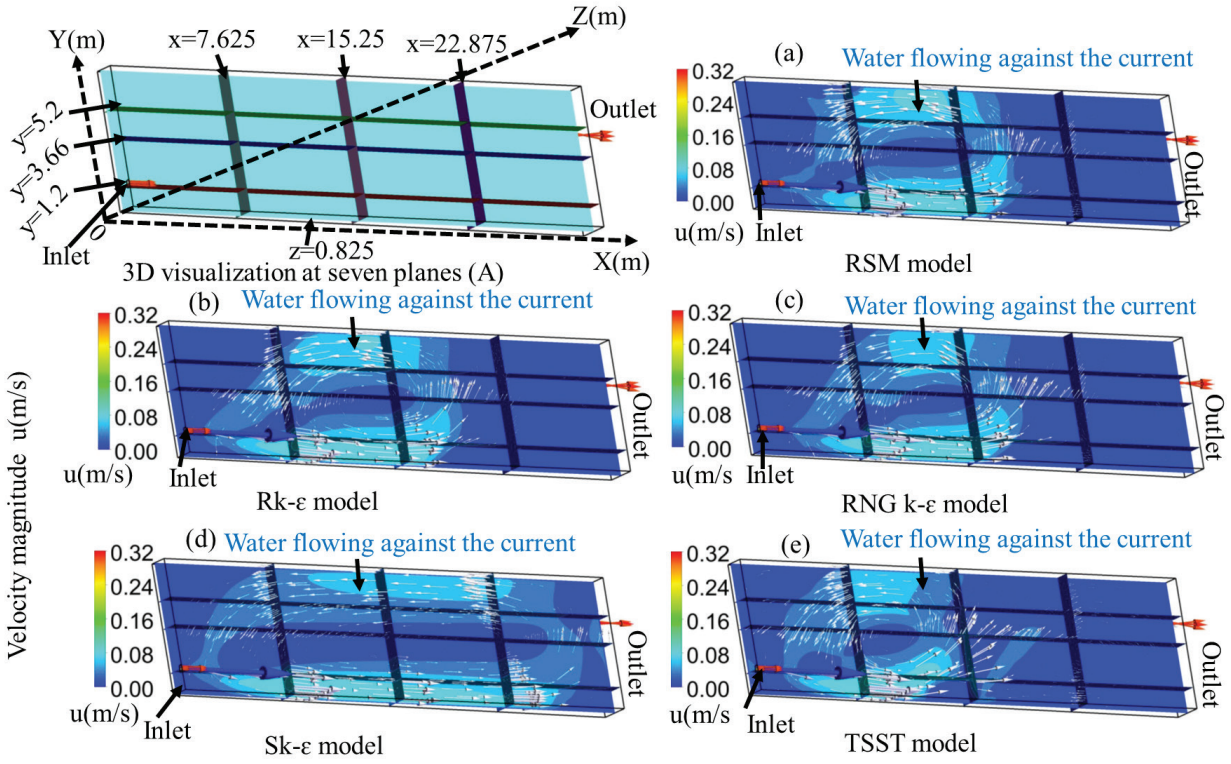

Fig. 4. Comparison of velocity contour and vectors at middle plane (z = 0.825 m), axial planes (y = 1.2m; y = 3.66 m; y = 5.2 m) and radial planes (x = 7.625 m; x = 15.25 m; x = 22.875 m) between the RSM, Rk-ε, RNG k-ε, Sk-ε and TSST models.

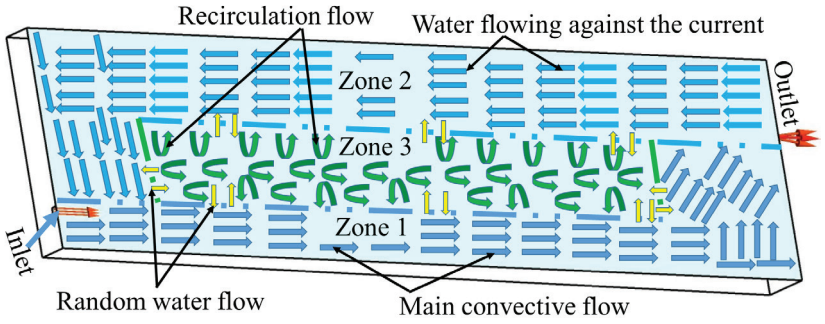

Fig. 5. Schematization of the global hydrodynamic behavior simulated by the 5 models.

- The first zone is located in the alignment of the inlet: the flow is directed from the inlet to the outlet. This zone is characterized by the convective acceleration of the water flow velocity that is due to the influence of the feed water jet at the inlet.
- The second zone is located in the outlet alignment: the flow is directed from the outlet to the inlet. It is the secondary current or backward flow zone with a direction opposite to that of the main current (zone 1).
- The third zone is located in the pond center between zones 1 and 2. This zone is characterized by the recirculation flow and low velocities.

The same hydrodynamic behavior sketched in Fig. 5 was observed by Alvarado et al. [62] in their inspection of velocity vectors in a waste water pond using only Sk-ε model. However, if the global behavior is similar for the five different turbulence models, numerous differences were observed at the local scale. The local velocity vector differs from one model to another. Inside the pond, the local velocity varies between $1.78.10^{-5}$ m/s and the maximum velocity fixed by the inlet flow (0.3 m/s). But the distribution of the different zones presented on Fig. 5 is not identical for all models. In the first zone, the flow appears predominantly convective according to the Sk-ε model (d), which is much less pronounced according to the other models. All models except Sk-ε predict a recirculation located in the upstream half of the pond. The recirculation is stretched along the whole pond with the Sk-ε model. Locally, the low flow rate (due to the low velocity distribution) is predominant from the axial middle to the downstream of the pond with the TSST model and RNG k-ε. The discrepancy observed in the local hydrodynamic behavior is due to the differences between the formulation hypotheses of the equations of each model or the effect of local Reynolds number [61,63].

3.1.2. Isosurfaces of velocity magnitude

An isosurface of velocity magnitude is a three-dimensional surface that represents all the points achieving the same constant value of the velocity magnitude within the pond volume. The mean flow velocity inside the pond is about 0.02 m/s for all models. We have determined an isosurface of velocity magnitude superior and inferior to the mean velocity in order to inspect the localization of lower and higher velocity inside the pond.

Fig. 6 shows the comparison of the isosurface of velocity magnitude equal to 0.03 m/s (superior to the mean velocity)

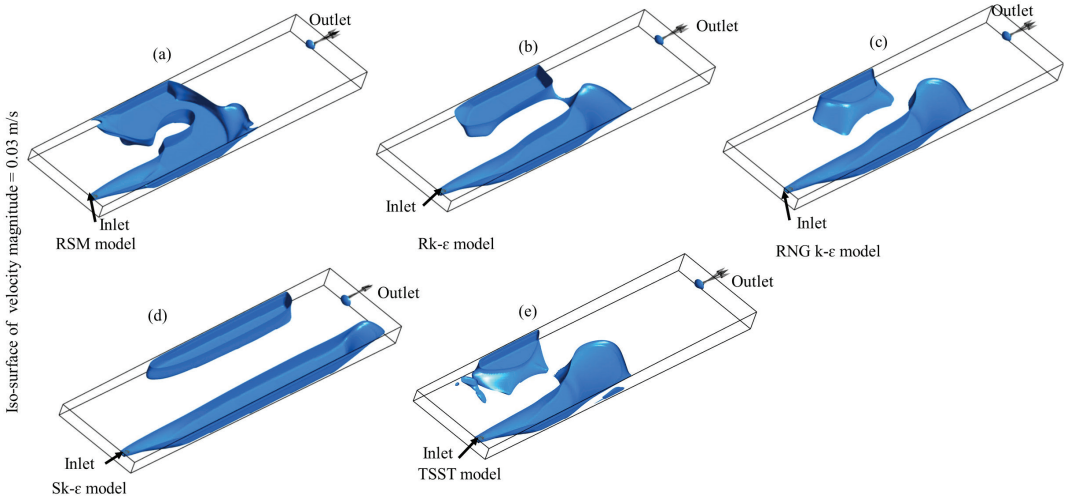

Fig. 6. Comparison of isosurfaces of velocity magnitude equal to 3.10^{-2} m/s between the 5 turbulence models. (a) RSM , (b) Rk-ε, (c) RNG k-ε, (d) Sk-ε and (e) TSST models.

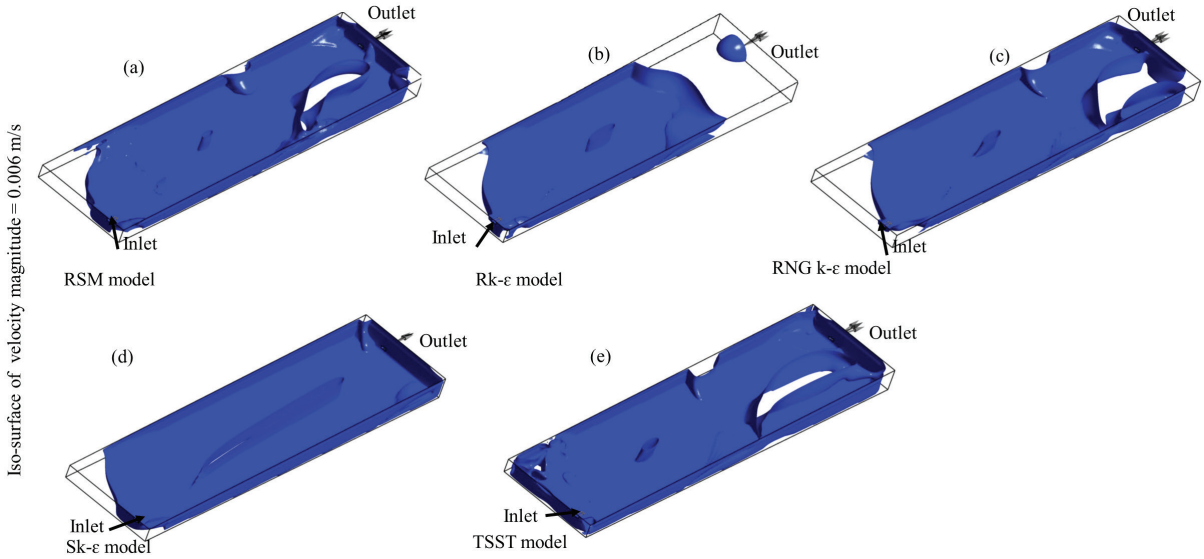

Fig. 7. Comparison of isosurfaces of velocity magnitude equal to 6.10^{-3} m/s between the 5 turbulence models. (a) RSM , (b) Rk-ε, (c) RNG k-ε, (d) Sk-ε and (e) TSST models.

between each model. We observed that the flow velocity value 0.03 m/s is mainly distributed upstream close to alignment of the inlet and around the pond center for the RSM (a), Rk-ε (b), RNG k-ε(c), and TSST (e) models. The shape of the resulting isosurfaces is almost similar for both models RNG k-ε (c) and TSST (e). But the forms of isosurfaces obtained with RSM (a), Rk-ε (b), and Sk-ε (d) models differ from one another.

Fig. 7 shows the comparison of isosurfaces of velocity magnitude equal to 0.006 m/s (inferior to the mean velocity) between each model. The isosurface is not spread enough downstream the pond for Rk-ε model. This shows that the location of lower velocity zone depends on the choice of the turbulence model.

3.2. *Influence of turbulence models on turbulence kinetic energy (k) prediction on a vertical line*

Fig. 8 shows the comparison of the turbulence kinetic energy (k) between the five turbulence models at a vertical line located at the position (x = 29.5 m; y = 5.2m) from the free surface to the pond bottom. It can be seen that Standard k-ε model predicts the highest turbulence kinetic energy compared to other four models. The gap of predicted of turbulence kinetic energy between Standard k-ε and Realizable k-ε is estimated at 28%. Compared to the three other models (RSM, RNG k-ε, and SST Transition), the gap is estimated at 25%. Wright et al. [63] compared the experimental and numerical results and found that the Standard k-ε model predicts the worst results of turbulence kinetic energy with an error of approximately 23% and the RNG k-ε gave values that were close to experimental measurement. The highest values of turbulent kinetic energy are caused by excessive estimation of the turbulence production term [63,64].

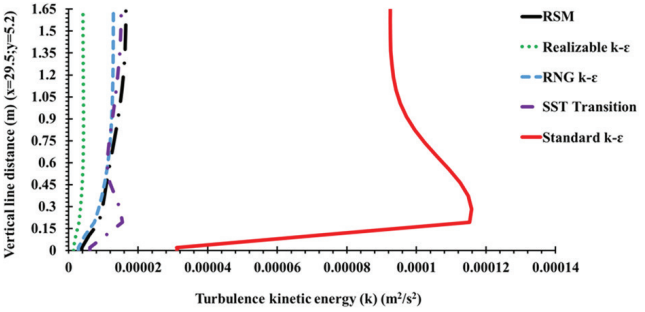

Fig. 8. Comparison of the turbulence kinetic energy (k) between the five turbulence models on a vertical line located at position (x = 29.5 m; y = 5.2 m).

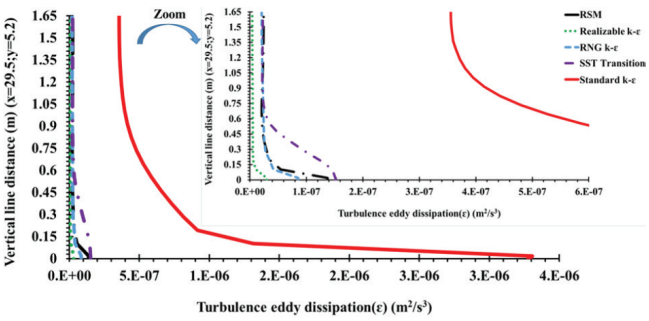

Fig. 9. Comparison of the turbulence eddy dissipation (ε) between the five turbulence models on a vertical line located at position (x = 29.5 m; y = 5.2m).

3.3. *Influence of turbulence models on turbulence eddy dissipation (ε) prediction on a vertical line*

Fig. 9 shows the comparison of the turbulence eddy dissipation (ε) between the five turbulence models at

vertical line located at the position (x = 29.5 m; y = 5.2 m). The Standard k-ε model appears to give significantly higher local values of the dissipation rate **(ε)** compared to other four models with a gap of 20%. The discrepancies observed explain why other alternative models have been developed to improve the equations of the turbulence parameters like turbulence eddy dissipation (ε) and the turbulence kinetic energy (k) [63,65,66]**.**

3.4. Influence of turbulence models on axial, transverse, and radial flow velocities

Several lines are defined in the pond in order to visualize the effect of the turbulence models on axial (x), transverse (y) and vertical (z) lines for steady flow, as shown in Fig. 10. These lines are chosen to approach roughly the main streamlines (lines that are tangent to the local velocity vectors; they represent the trajectory of massless particle moving with the water flow).

The prediction of the local flow with each of the models is dependent on the variation of the local Reynolds number which is dependent on the mean local velocity. Aside from the RNG k-ε and Transition SST models, the other three models (RSM, Rk-ε, Sk-ε) have been developed mainly for turbulent flows with high Reynolds number. The variation of the local Reynolds number will involve the influences of the axial, transverse, and vertical flow velocities simulated by the five turbulence models in areas where the flow has a low Reynolds number.

Fig. 11a shows a comparison of the local velocity magnitude on the axial line located on the free surface in the alignment of the inlet between the RSM, Rk-ε, RNG k-ε, Sk-ε, and Transition SST models. This line is located in zone 1 (Fig. 5), where the flow is mainly convective. The five turbulence models predict almost the same value of velocity magnitude from inlet (upstream) to the middle length of the pond.

The five turbulences models predicted approximately the same value of velocity magnitude from inlet (upstream) to the middle length of the pond. But we observed some discrepancy in the part between the middle length and the downstream end because of the influence of recirculation and lower velocity near this area. Compared to the other four

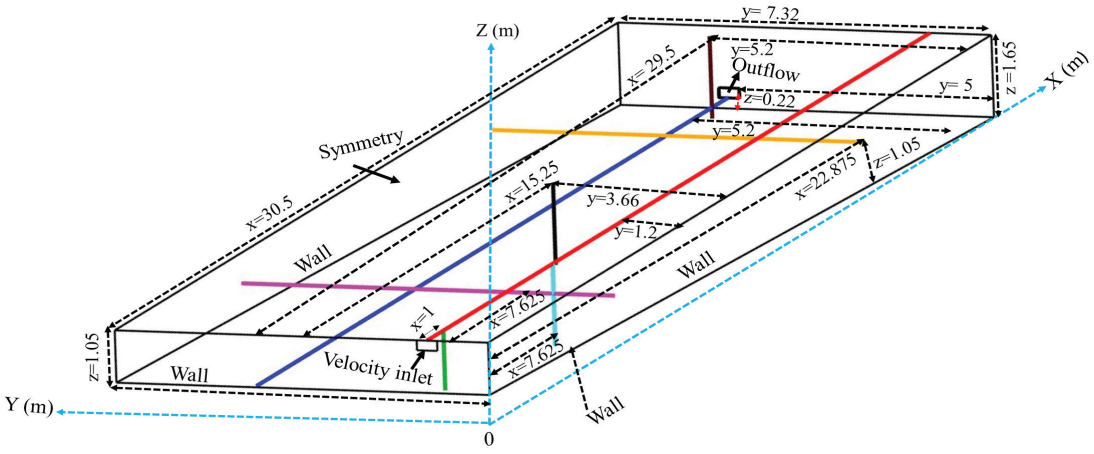

Fig. 10. Location of axial, transverse and vertical lines used for velocity profile comparison between the 5 models.

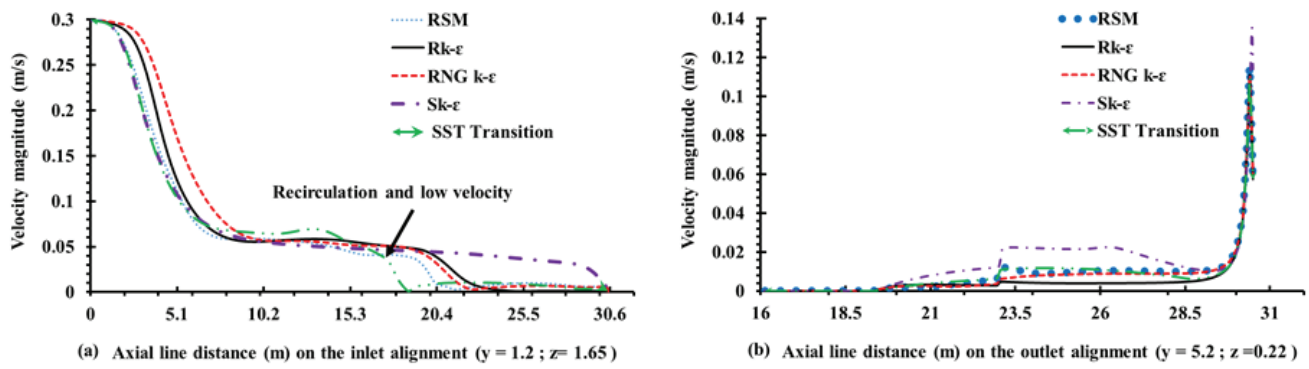

Fig. 11. Comparison of velocity profiles on axial lines (a)/(y = 1.2 ; z = 1.65) and (b)/(y = 5.2 ; x = 0.22) between the RSM , Rk-ε, RNG k-ε, Sk-ε and TSST models.

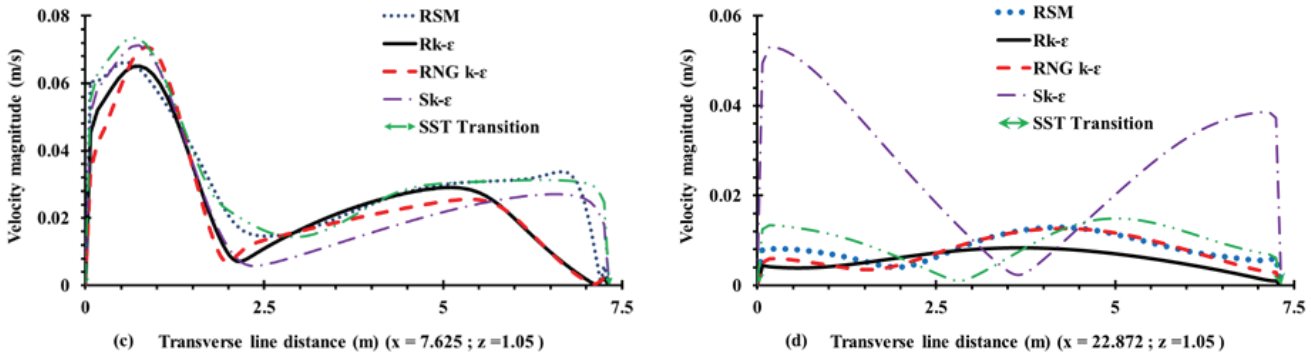

Fig. 12. Comparison of velocity profiles on transverse lines (c)/(x = 7.625; z = 1.05) and (d)/(x = 22.872 ; z = 1.05) between the RSM, Rk-ε, RNG k-ε, Sk-ε and TSST models.

models, the Transition SST model detects earlier a low flow velocity on these axial lines because of its ability to capture areas of laminar-turbulent-transitional regime.

Fig. 11b shows a comparison of the velocity magnitude on the axial line located at middle depth on the pond center between the RSM, Rk-ε, RNG k-ε, Sk-ε, and TSST models. We remark that near the high recirculation area, the Sk-ε model predicted higher velocity because of the highest value of turbulence kinetic energy (k) predicted by this model [31,63]. Then, we observe that the area where there is more influence of turbulence models on longitudinal flow is the area between the pond centers following the longitude and the downstream as shown in Fig. 10.

Fig. 12c shows a comparison of velocity magnitude on the transverse line located at 0.6 m (about one-third of the depth) from the free surface and at 7.625 m (a quarter of the length of the pond) from the upstream end. This line crosses successively zones 1, 2, and 3 (Figs. 5 and 10). We have found the same tendency of velocity evolution on this line for the five models apart from zone 3 (from 5.2 m to 7.32 m following the transverse direction).

Fig. 12d shows a comparison of velocity magnitude on transverse line located at 7.625 m (three-quarters of the pond length) from the inlet and at 0.6 m (about one-third of the depth) of the free surface. Compared to the four other models, the Standard k-ε model predicts a high flow velocity. Jacobs et al. [67] also found in the water flow simulation that the Standard k-ε model predicted a 28% increase of the flow velocity compared to four other models (RNG k-ε, Realizable k-ε, SST k-ω and Standard k-ω) and the experimental velocity measurements.

Inside ponds, natural phenomena (sedimentation, biological cycle, from photosynthesis to biodegradation) occur preferentially in the vertical direction. The vertical flows hence play an important role in the understanding of these phenomena. Therefore, it is important to inspect the influence of the models on the velocity magnitude profiles. Fig. 13 shows the effect of the five turbulence models on velocity profiles on vertical lines located in different positions from the free surface to the bottom. Whatever the position of the vertical line, the five models simulated a decreasing flow rate from the free surface to the bottom. On the vertical line located at 1 m from the inlet (Fig. 13e), the five models give almost the same results of velocity profiles because in this area the range of local Reynolds number is suitable for all models. The further we go away from the inlet, the more we see the differences between the five models because some models do not fully capture the hydrodynamics of transitional Reynolds number values (Fig. 13f–h). We note that on the vertical line in the center of the pond, the TSST model simulates a significant different velocity magnitude compared to other four models (Fig. 13g). On the vertical line located at 1 m of the outlet, we observed three tendencies of flow velocity behavior: the Rk-ε and the Sk-ε models predicted, respectively, a low and higher flow velocity, and the three other models (RSM, RNG k-ε, and TSST) predict a similar velocity evolution (Fig. 13h).

3.5. Influence of the turbulence model on the RTD

In order to have a more comprehensive description of the flow in the pond and to validate the simulations, numerical tracing (using a species transport method) was performed to determine the RTD. In this approach, the simulated tracer is injected from the inlet at t = 0 second. The influence of the turbulence model on RTD is inspected. Fig. 14 shows a comparison of the RTD obtained with the five turbulence models (RSM, Rk-ε, RNG k-ε, Sk-ε and TSST models).

The five turbulence models simulate overall the same hydrodynamic behavior and they should give almost the same MRT values, which is confirmed in Table 4. The most interesting aspect is the differences on the second-order moment reflected by the different shapes (Fig. 14). At the outlet of the pond, the five turbulence models detect the maximum concentration of the simulated tracer at the following flow times: 15 minutes for the Sk-ε model, 26 minutes for the RSM model, 30 minutes for RNG k-ε model, 34 minutes for the SST Transition model, and 41 minutes for the Rk-ε model. The Sk-ε model predicts an accelerated outflow (strong short-circuiting) of the tracer with a peak of concentration, at least twice as high as the four other models. The discrepancies of peak concentration between the four other models (RSM, Rk-ε, RNG k-ε, and TSST models) are low.

A portion of the numerical tracer is transported by the flow inside the pond by the recirculation phenomena, the flow velocity and the molecular diffusion. Since the flow is very slow within a pond, a portion of the tracer puts

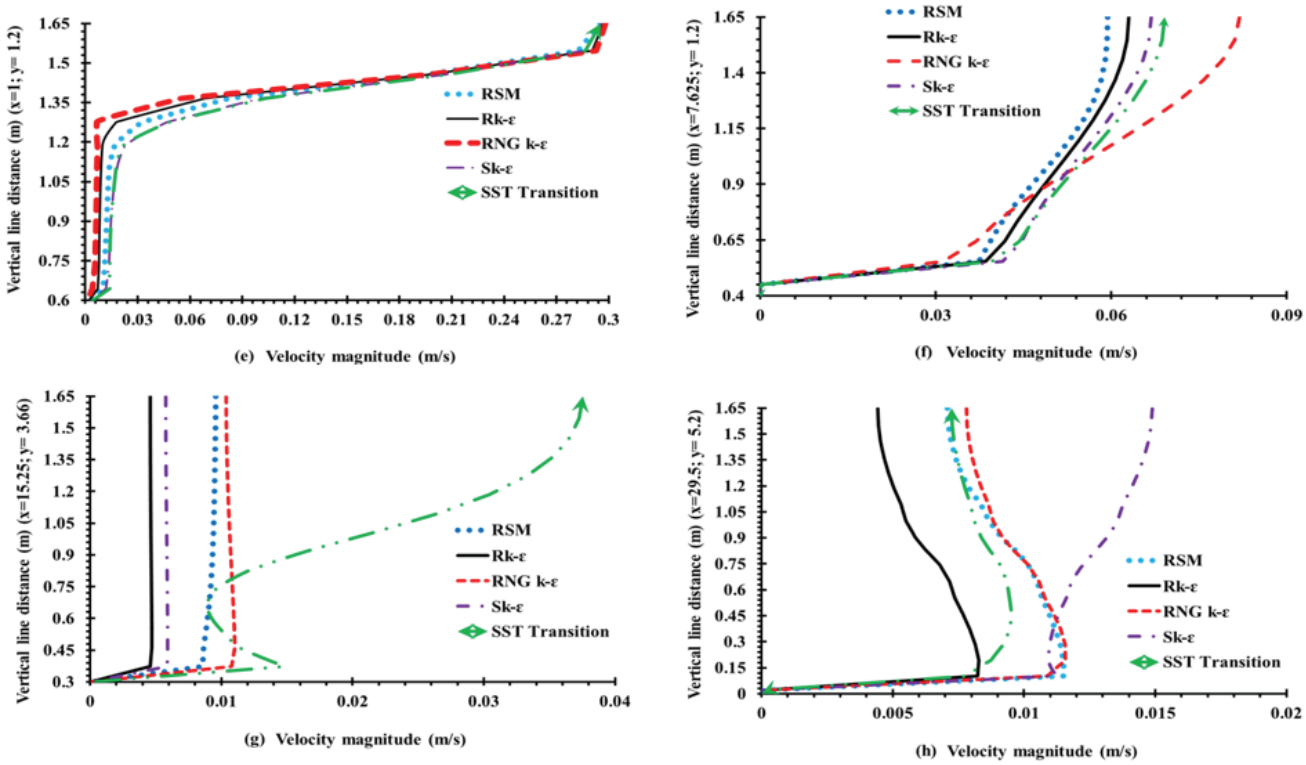

Fig. 13. Comparison of velocity profiles on vertical lines (e)/(x = 1 ; y = 1.2), (f)/(x = 7.625 ; y = 1.2), (g)/(x = 15.25; y = 3.66), (h)/(x = 29.5; y = 5.2) between the RSM , Rk-ε, RNG k-ε, Sk-ε and Transition SST models.

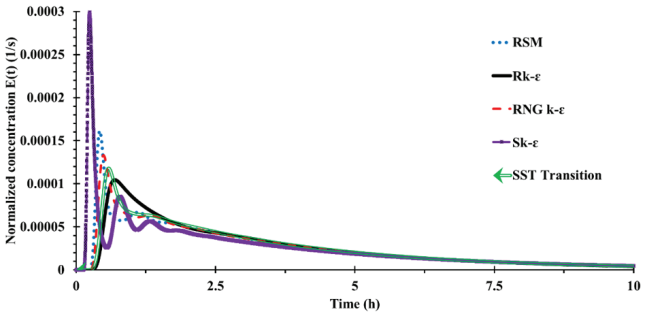

Fig. 14. Comparison of Residence Time Distribution between the five turbulence models.

Table 4
Comparison of theoretical and numerical Mean Residence Time (MRT)

MRT (hours)	Theoretical	RSM	Rk-ε	RNG k-ε	Sk-ε	TSST
	3.49	3.51	3.49	3.52	3.53	3.55

enough time within the pond because of low flow velocity and the stagnant zone. This portion of the tracer is affected by the dilution and homogenization with the continuous medium (water) after a period longer than the MRT. The five models predict almost the same low concentration values approximately 2 hours after numerical tracer injection because of the effect of dilution or homogenization of numerical tracer concentration inside the pond.

3.6. Influence of the turbulence model on concentration of substance dispersion inside the pond

The dispersion of an active substance was simulated by numerical injection of a substance at a point where the flow velocity is very low (at the center of the pond, on the free surface). The area of the injection point was targeted for local treatment due to the invasion of invasive plants at low flow velocity zone [68–70]. Fig. 15 shows the comparison of concentration dispersion on the free surface, 3 minutes after injection, between the five turbulence models. The numerical tracer dispersion inside the pond is dependent on the advection also called convection, turbulent diffusion, and molecular diffusion. At the injection location, there is a progressive decrease of the tracer concentration. In Fig. 15a, the RSM model predicted extreme values of mass fraction of the substance between 0 and 2.4 x 10^{-3}. Compared to the RSM model, the Standard k-ε predicted the same value of mass fraction while the Realizable k-ε, the RNG k-ε, and the SST Transition give, respectively, a gap of 70%, 22%, and 14%. The direction of the concentration dispersion appears to differ from one model to another.

Fig. 16 shows the comparison of concentration dispersion (of the simulated tracer injected at the center of the pond, on the free surface) at the middle horizontal plane at flow time equal to 21.1 minutes between the five models. The Rk-ε (Fig. 16b)

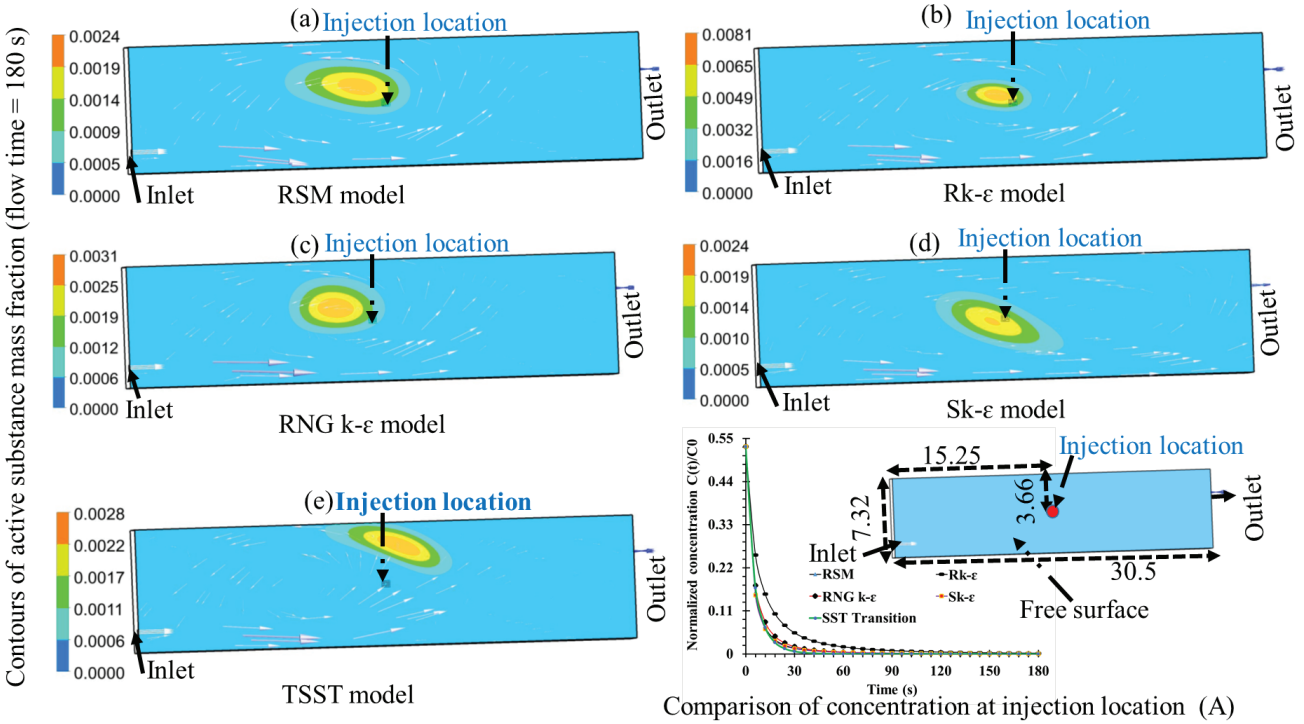

Fig. 15. Comparison of concentration dispersion at the free surface between (a) RSM, (b) Rk-ε, (c) RNG k-ε, (d) Sk-ε and (e) TSST models.

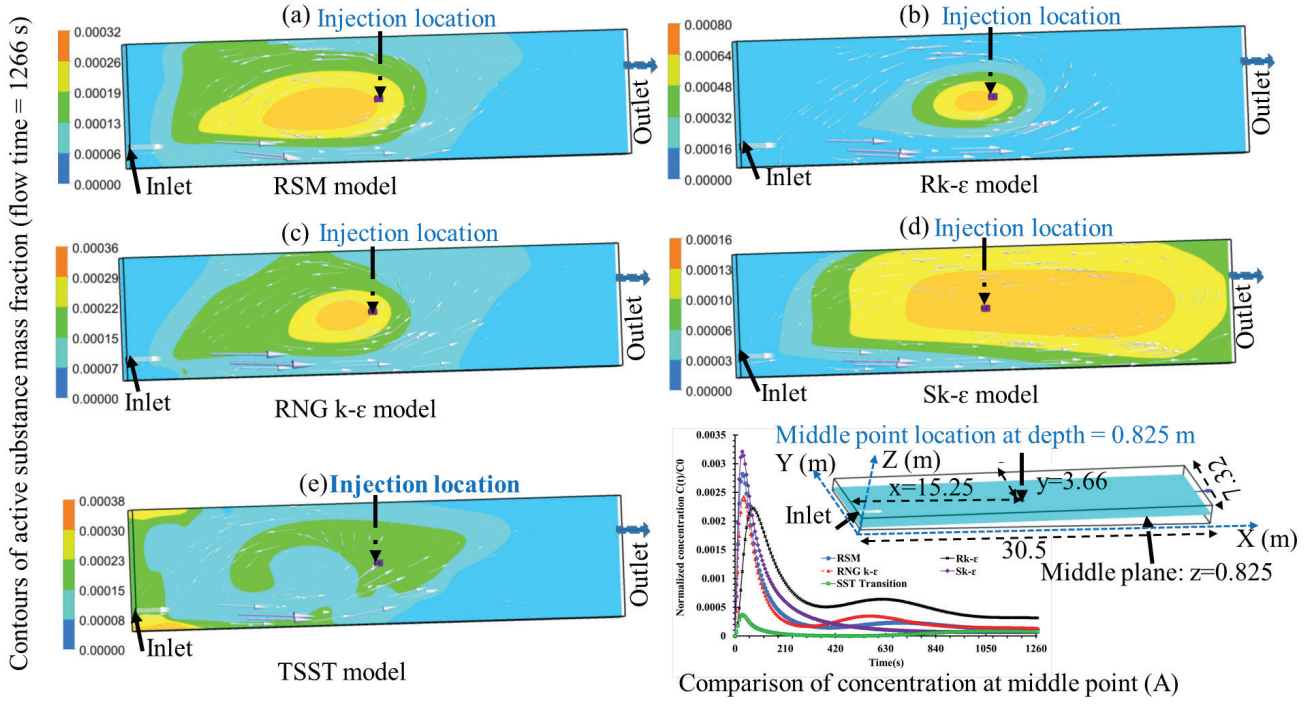

Fig. 16. Comparison of concentration dispersion at the middle horizontal plane (z = 0.825) between (a) RSM, (b) Rk-ε, (c) RNG k-ε, (d) Sk-ε and (e) TSST models.

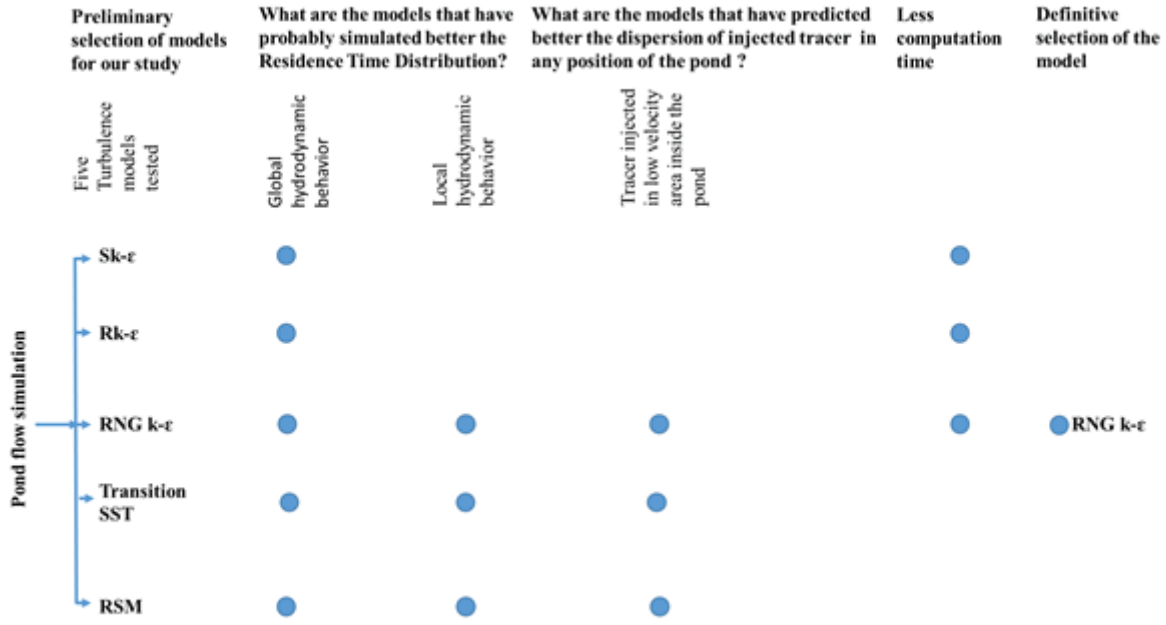

Fig. 17. Simple strategy for the definitive selection of the model.

model predicts slow concentration dispersion while the Sk-ε model (Fig. 16d) predicts a large dispersion. At this time, the RSM (Fig. 16a) model predicted extreme values of mass fraction of substance which is between 0 and 3.6 x 10^{-4} with the gap of 56% compared to the mass fraction detected at 3 minutes. Compared to the RSM model, the Standard k-ε, the Realizable k-ε, the RNG k-ε, and the SST Transition give, respectively, the gap of 50%, 55%, 11% and 16%.

Only the TSST model (Fig. 16e) predicts that the tracer disperses onto the bank upstream at flow time 21.1 minutes. The monitoring of the simulated tracer concentration at a point located at a mid-depth in the same level as the injection point following the vertical shows that the concentration at this point is estimated lower by the TSST model (curve in Fig. 16a) compared to the other models. This result shows clearly the strong impact on the prediction of active substance concentration in the pond.

3.7. Model selection criterion

Fig. 17 shows the simple strategy for the definitive selection of the model. The selection is based on the criteria of the RTD, analysis of the local hydrodynamic behavior, the local dispersion of the tracer injected in low velocity area and less computation time. The computation time (on an Intel Core computer, with a 3.20 GHz i3 4-processor and 4 GB RAM) of pond flow simulation after 20,000 iterations is approximately 7–12 hours for the k-ε family model (Sk-ε, Rk-ε, RNG k-ε), 30 hours for transition SST k-ω model and 40 hours for RSM the model. Compared to the four other models, RNG k-ε fulfills all these conditions as shown in Fig. 17.

4. Conclusions

The flow visualization inside the pond shows that the global predicted hydrodynamic behavior is similar for these five turbulence models (RSM, Rk-ε, RNG k-ε, Sk-ε, and Transition SST models). However, each of the five turbulence models predicts differently the local hydrodynamic behavior in slow flow areas inside the pond where algae could be localized. These differences are reflected on the shape of the RTD curve which confirms the interest of tracer experiment when it is possible. The isosurfaces of velocity magnitude simulated by Sk-ε model indicate a flow with a strong short-circuiting. The low velocity distribution in stagnant areas simulated by Rk-ε model is different from other four models. Among all turbulence models, Standard k-ε model appears to give significantly higher local values of the turbulence kinetic energy (k) and the dissipation rate (ε) which affects the local flow velocity and the peak concentration prediction. The dispersion monitoring of the active substance tracer which is injected at a position located within the pond (in a low-velocity area) shows that the choice of turbulence model also affects the local dispersion.

A detailed analysis of the results allows to select the most adapted model without complex (and sometime impossible) tracer experiments in real pool. We can assume that the RSM and RNG k-ε models provide better results for the local hydrodynamic behavior with local recirculation and stagnant zones than the Rk-ε and Sk-ε models. We found that the Transition SST model promotes the dispersion of injected tracer in the areas nearest the walls compared to the four other models. Based on the physical analysis of local flow behavior and reasonable computational time, RNG k-ε was selected as the definitive model for the simulation of pond hydrodynamic behavior.

Acknowledgements

This research was undertaken as a part of BioCapTech project funded by the Agency for Economic Mobilization (AME) of the Regional Council of Lorraine and the European Regional Development Fund (ERDF) to which the authors express their sincere thanks.

Nomenclature

CFD — Computational fluid dynamics
$D_{i,m}$ — Diffusion coefficient for species i in the mixture, m^2/s
D_t — Turbulent diffusion, m^2/s
FAO — Food and Agriculture Organization
I — Turbulent intensity, dimensionless
k — Turbulent kinetic energy, m^2/s^2
MRT — Mean residence time, s
p — Static pressure, Pa
Re — Reynolds number, dimensionless
Rk-ε — Realizable k-epsilon
RNG — Re-Normalization Group
RSM — Reynolds Stress Model
RTD — Residence time distribution
Sc_t — Turbulent Schmidt number, dimensionless
Sk-ω — Standard k-omega
Sk-ε — Standard k-epsilon
SST — Shear-Stress Transport
t — Time, s
TSST — Transition Shear Stress Transport
U — Mean flow velocity, m/s
u — Instantaneous velocity, m/s
u_i',u'_j — Turbulent velocity fluctuation, m/s
Y_i — Local mass fraction of each species, dimensionless
x, y, z — Directional components, m

Greek symbols

ε — Dissipation rate of the turbulent kinetic energy, m^2/s^3
ϱ — Density, kg/m^3
ω — Specific dissipation rate, 1/s
ν — Kinematic viscosity, m^2/s

References

[1] P. De Schryver, A.K. Sinha, P.S. Kunwar, K. Baruah, W. Verstraete, N. Boon, G. De Boeck and P. Bossier, Poly-β-hydroxybutyrate (PHB) increases growth performance and intestinal bacterial range-weighted richness in juvenile European sea bass, *Dicentrarchus labrax*, Appl. Microbiol. Biot., 86 (2010) 1535–1541.
[2] D.W. Schindler, Recent advances in the understanding and management of eutrophication, Limnol. Oceanogr., 51 (2006) 356–363.
[3] Z.-G. Ji, Hydrodynamics and Water Quality: Modeling Rivers, Lakes, and Estuaries, John Wiley & Sons, Hoboken, New Jersey, 2007.
[4] J. Laurent, R.W. Samstag, J.M. Ducoste, A. Griborio, I. Nopens, D.J. Batstone, J.D. Wicks, S. Saunders and O. Potier, A protocol for the use of computational fluid dynamics as a supportive tool for wastewater treatment plant modelling, Water Sci. Technol., 70 (2014) 1575.
[5] I.-B. Lee, J.P.P. Bitog, S.-W. Hong, I.-H. Seo, K.-S. Kwon, T. Bartzanas and M. Kacira, The past, present and future of CFD for agro-environmental applications, Comp. Electron. Agriculture, 93 (2013) 168–183.
[6] R.E. Burrows and H.H. Chenoweth, Evaluation of Three Types of Fish Rearing Ponds Evaluation of Three Types of Fish Rearing Ponds, Vol. 39, US Government Printing Office, Washington D.C., 1955.
[7] M.B. Timmons, S.T. Summerfelt and B.J. Vinci, Review of circular tank technology and management, Aquacult. Eng., 18 (1998) 51–69.
[8] J. Oca and I. Masalo, Flow pattern in aquaculture circular tanks: Influence of flow rate, water depth, and water inlet & outlet features, Aquacult. Eng., 52 (2013) 65–72.
[9] S.T. Summerfelt, J. Davidson, G. Wilson and T. Waldrop, Advances in fish harvest technologies for circular tanks, Aquacult. Eng., 40 (2009) 62–71.
[10] C.S. Tucker and J.A. Hargreaves, Environmental Best Management Practices for Aquaculture, John Wiley & Sons, Hoboken, New Jersey, 2009.
[11] E. Carballo, A. van Eer, T. Van Schie and A. Hilbrands, Small-Scale Freshwater Fish Farming, Agromisa Foundation and CTA, Wageningen, The Netherlands, 2008.
[12] O.-I. Lekang, Aquaculture Engineering, John Wiley & Sons, Hoboken, New Jersey, 2013.
[13] M.P. Masser and J.W. Jensen, Calculating Area and Volume of Ponds and Tanks, Southern Regional Aquaculture Center, Stoneville, Mississippi, 1991.
[14] J. Oca and I. Masaló, Design criteria for rotating flow cells in rectangular aquaculture tanks, Aquacult. Eng., 36 (2007) 36–44.
[15] F. Paezosuna, Shrimp aquaculture development and the environment in the Gulf of California ecoregion, Mar. Pollut Bull., 46 (2003) 806–815.
[16] E.L. Peterson, Observations of pond hydrodynamics, Aquacult. Eng., 21 (2000) 247–269.
[17] J. Davidson and S. Summerfelt, Solids flushing, mixing, and water velocity profiles within large (10 and 150 m^3) circular "Cornell-type" dual-drain tanks, Aquacult. Eng., 32 (2004) 245–271.
[18] C.-W. Bi, Y.-P. Zhao, G.-H. Dong, Y.-N. Zheng and F.-K. Gui, A numerical analysis on the hydrodynamic characteristics of net cages using coupled fluid–structure interaction model, Aquacult. Eng., 59 (2014) 1–12.
[19] S. Delaux, C.L. Stevens and S. Popinet, High-resolution computational fluid dynamics modelling of suspended shellfish structures, Environ. Fluid. Mech., 11 (2011) 405–425.
[20] D.L. Huggins, R.H. Piedrahita and T. Rumsey, Use of computational fluid dynamics (CFD) for aquaculture raceway design to increase settling effectiveness, Aquacult. Eng., 33 (2005) 167–180.
[21] D.L. Huggins, R.H. Piedrahita and T. Rumsey, Analysis of sediment transport modeling using computational fluid dynamics (CFD) for aquaculture raceways, Aquacult. Eng., 31 (2004) 277–293.
[22] R.A. Labatut, J.M. Ebeling, R. Bhaskaran and M.B. Timmons, Modeling hydrodynamics and path/residence time of aquaculture-like particles in a mixed-cell raceway (MCR) using 3D computational fluid dynamics (CFD), Aquacult. Eng., 67 (2015) 39–52.
[23] R.A. Labatut, J.M. Ebeling, R. Bhaskaran and M.B. Timmons, Exploring flow discharge strategies of a mixed-cell raceway (MCR) using 2-D computational fluid dynamics (CFD), Aquacult. Eng., 66 (2015) 68–77.
[24] J.H. Montas, G.V.S. Prabhakar and F. Wheaton, CFD analysis of flow in aquaculture tanks. Proceedings of the 93rd Annual International Meeting of ASAE. Biological Resources Engineering Department. University of Maryland at College Park, 9–12 July. ASAE paper No 003111, (2000) 1–24.
[25] A. Alvarado, M. Vesvikar, J.F. Cisneros, T. Maere, P. Goethals and I. Nopens, CFD study to determine the optimal configuration of aerators in a full-scale waste stabilization pond, Water Res., 47 (2013) 4528–4537.
[26] B. Wu and Z. Chen, An integrated physical and biological model for anaerobic lagoons, Bioresource Technol., 102 (2011) 5032–5038.
[27] V.R. Stovin, J.P. Grimm and S.-T.D. Lau, Solute Transport Modeling for Urban Drainage Structures, J. Environ. Eng.-ASCE, 134 (2008) 640–650.

[28] J. Kim, P. Moin and R. Moser, Turbulence statistics in fully developed channel flow at low Reynolds number, J. Fluid Mech., 177 (1987) 133–166.
[29] I. Marusic, D.D. Joseph and K. Mahesh, Laminar and turbulent comparisons for channel flow and flow control, J. Fluid Mech., 570 (2007) 467.
[30] B. Wu and S. Chen, CFD simulation of non-Newtonian fluid flow in anaerobic digesters, Biotechnol. Bioeng., 99 (2008) 700–711.
[31] E. Furbo, Evaluation Of RANS Turbulence Models For Flow Problems With Significant Impact of Boundary Layers, M.Sc. Thesis, Uppsala University, Sweden, 2010).
[32] W. Wu, P. Wang and N. Chiba, Comparison of five depth-averaged 2-D turbulence models for river flows, Arch. Hydro-eng. Environ. Mechanics, 51 (2004) 183–200.
[33] M.-L. Zhang, C.W. Li and Y.-M. Shen, A 3D non-linear k–ε turbulent model for prediction of flow and mass transport in channel with vegetation, Appl. Math. Model., 34 (2010) 1021–1031.
[34] M.P. Bulat and P.V. Bulat, Comparison of turbulence models in the calculation of supersonic separated flows, World App. Sci., J. 27 (2013) 1263–1266.
[35] E.C. Douvi, A.I. Tsavalos and D.P. Margaris. Evaluation of the turbulence models for the simulation of the flow over a National Advisory Committee for Aeronautics (NACA) 0012 airfoil, J. Mech. Eng. Res., 4 (2012)100-111.
[36] T.S.D. Karthik and F. Durst, Turbulence Models and Their Applications, Department of Mechanical Engineering, Indian Institute of Technology, Madras, India, 2011.
[37] F. Rostami, M. Shahrokhi, M.A. M.A.M. Said, R. Abdullah and Syafalni, Numerical modeling on inlet aperture effects on flow pattern in primary settling tanks, Appl. Math. Model., 35 (2011) 3012–3020.
[38] A. Yakhot, S.A. Orszag, V. Yakhot and M. Israeli, Renormalization group formulation of large-eddy simulations, J. Sci. Comput., 4 (1989) 139–158.
[39] B.E. Launder, G.J. Reece and W. Rodi, Progress in the development of a Reynolds-stress turbulence closure, J. Fluid Mech., 68 (1975) 537–566.
[40] L.N. Robinson, Water Resources Research Progress, Nova Publishers, New York, New Jersey, 2008.
[41] F.R. Menter, R.B. Langtry, S.R. Likki, Y.B. Suzen, P.G. Huang and S. Völker, A correlation-based transition model using local variables—Part I: Model formulation. J. Turbomach., 128 (2006) 413-422.
[42] Ansys Fluent, Ansys Fluent Theory Guide. http://www.ansys.com, visited on Oct. 1, 2013.
[43] W.H. Graf, Fluvial Hydraulics, John Wiley & Sons Ltd, Hoboken, New Jersey, 1998.
[44] S. Khatiwala, M. Visbeck and M.A. Cane, Accelerated simulation of passive tracers in ocean circulation models, Ocean Model., 9 (2005) 51–69.
[45] D. Kim, D.-I. Kim, J.-H. Kim and T. Stoesser, Large eddy simulation of flow and tracer transport in multichamber ozone contactors, J. Environ. Eng.-ASCE, 136 (2009) 22–31.
[46] W. Rauen, B. Lin, R. Falconer and E. Teixeira, CFD and experimental model studies for water disinfection tanks with low Reynolds number flows, Chem. Eng. J., 137 (2008) 550–560.
[47] B. Andersson, Ed., Computational Fluid Dynamics for Engineers, Cambridge University Press, Cambridge, New York, 2012.
[48] A. Alvarado, S. Vedantam, G. Durazno and I. Nopens, Hydraulic assessment of waste stabilization ponds: Comparison of computational fluid dynamics simulations against tracer data, MASKANA, 2(1) (2011) 81-89.
[49] L. Nastac, L. Zhang, B.G. Thomas, A. Sabau, N. El-Kaddah, A.C. Powell and H. Combeau, CFD Modeling and Simulation in Materials Processing, John Wiley & Sons, Hoobken, New Jersey, 2012.
[50] M. Ahsan, Numerical analysis of friction factor for a fully developed turbulent flow using k–ε turbulence model with enhanced wall treatment, J. Basic Appl. Sci., 3 (2014) 269–277.
[51] A.M. Goula, M. Kostoglou, T.D. Karapantsios and A.I. Zouboulis, A CFD methodology for the design of sedimentation tanks in potable water treatment, Chem. Eng. J. 140 (2008) 110–121.
[52] M.-H. Chung, An adaptive Cartesian cut-cell/level-set method to simulate incompressible two-phase flows with embedded moving solid boundaries, Comput. Fluids, 71 (2013) 469–486.
[53] W.J. Coirier, An adaptively-refined, Cartesian, cell-based scheme for the Euler and Navier-Stokes equations, Ph.D. thesis, University of Michigan, Ann Arbor, Michigan, USA.
[54] M.W. Johnson, A novel Cartesian CFD cut cell approach, Comput. Fluids, 79 (2013) 105–119.
[55] J. Karcz and L. Kacperski, An effect of grid quality on the results of numerical simulations of the fluid flow field in an agitated vessel, In: Proceedings 14th European conference on mixing, Warszawa, 2012.
[56] T. Frank, C. Lifante, H.-M. Prasser and F. Menter, Simulation of turbulent and thermal mixing in T-junctions using URANS and scale-resolving turbulence models in ANSYS CFX, Nucl. Eng. Des., 240 (2010) 2313–2328.
[57] T.X. Ho, P. Kosinski, A.C. Hoffmann and A. Vik, Numerical modeling of solid oxide fuel cells, Chem. Eng. Sci., 63 (2008) 5356–5365.
[58] M. Karimi, G. Akdogan, S.M. Bradshaw, Effects of different mesh schemes and turbulence models in CFD modelling of stirred tanks, Physicochem. Probl. Mi., 48 (2012) 513–531.
[59] X. Liu and G. Parker, Modeling of Hydrodynamics and Sediment Transport in St. Clair River, Report SD-12 of the St. Clair River Task Team for the International Upper Great Lakes Study, International Joint Commission (2009).
[60] A.R. Coughtrie, D.J. Borman and P.A. Sleigh, Effects of turbulence modelling on prediction of flow characteristics in a bench-scale anaerobic gas-lift digester, Bioresource Technol., 138 (2013) 297–306.
[61] G. Eggenspieler, Turbulence modeling, ANSYS Inc. Canonsburg, Pennsylvania, 2012.
[62] A. Alvarado, S. Vedantam, P. Goethals and I. Nopens, A compartmental model to describe hydraulics in a full-scale waste stabilization pond, Water Res., 46 (2012) 521–530.
[63] N.G. Wright and G.J. Easom, Non-linear k–ε turbulence model results for flow over a building at full-scale, Appl. Math. Model., 27 (2003) 1013–1033.
[64] B. Merci, B. Naud and D. Roekaerts, Flow and mixing fields for transported scalar PDF simulations of a piloted jet diffusion flame ("Delft Flame III"), Flow Turbul. Combust., 74 (2005) 239–272.
[65] P.L. Davis, A.T. Rinehimer and M. Uddin, A comparison of RANS-based turbulence modeling for flow over a wall-mounted square cylinder, In: Proceeding 20th Annual Conference of the CFD Society of Canada, 2012.
[66] R. Peyret and E. Krause, Advanced Turbulent Flow Computations, Springer, Vienna, Austria, 2014.
[67] C. Jacobs, Z. Qin and K. Bremhorst, Comparison of RANS modelling with DNS and experimental data for a converging-diverging nozzle and a rotating cylinder electrode, In: Fifth International Conference on CFD in the Process Industries, 400 (2006) 1–6.
[68] E. Vernon and H. Hamilton, Literature review on methods of control and eradication of Canadian pondweed and Nuttall's pondweed in standing waters. Scottish Natural Heritage Commissioned Report No. 433, 2011.
[69] J.M. Evans, Ecosystem implications of invasive aquatic plants and aquatic plant control in Florida springs, Summary and synthesis of the available literature on the effects of nutrients on spring organisms and systems, University of Florida Water Institute, Gainesville, Florida, (2008) 231–270.
[70] R.J. Rolls, C. Leigh and F. Sheldon, Mechanistic effects of low-flow hydrology on riverine ecosystems: ecological principles and consequences of alteration, Freshwater Sci., 31 (2012) 1163–1186.
[71] R. Tarpagkou and A. Pantokratoras, CFD methodology for sedimentation tanks: The effect of secondary phase on fluid phase using DPM coupled calculations, Appl. Math. Model., 37 (2013) 3478–3494.
[72] R. Hreiz, B. Sialve, J. Morchain, R. Escudié, J.-P. Steyer and P. Guiraud, Experimental and numerical investigation of hydrodynamics in raceway reactors used for algaculture, Chem. Eng. J., 250 (2014) 230–239.